Available online at www.sciencedirect.com
SCIENCE DIRECT®
Journal of Solid State Chemistry 178 (2005) 1395–1405
JOURNAL OF SOLID STATE CHEMISTRY
www.elsevier.com/locate/jssc

Comparative study of sol–gel-hydrothermal and sol–gel synthesis of titania–silica composite nanoparticles

Zhijie Li[a,b], Bo Hou[a,b], Yao Xu[a], Dong Wu[a], Yuhan Sun[a,*], Wei Hu[c], Feng Deng[c]

[a]*State Key Laboratory of Coal Conversion, Institute of Coal Chemistry, Chinese Academy of Sciences, Taiyuan 030001, China*
[b]*Graduate School of Chinese Academy of Sciences, Beijing 100039, China*
[c]*State Key Laboratory of Magnetic Resonance and Atomic Molecular Physics, Institute of Physics and Mathematics, Chinese Academy of Sciences, Wuhan 430071, China*

Received 17 November 2004; received in revised form 20 December 2004; accepted 26 December 2004
Available online 16 March 2005

Abstract

Titania–silica composite nanoparticles were prepared by sol–gel-hydrothermal and sol–gel routes, respectively, and their physicochemical and photocatalytic properties were compared. The results of XRD, TEM and BET surface areas showed that sol–gel-hydrothermal route led to anatase titania–silica composite nanoparticles with large specific surface area, but the sol–gel route tended to form mixture of anatase and rutile. The composite nanoparticles prepared by sol–gel-hydrothermal route had better thermal stability against phase transformation from anatase to rutile, agglomeration and particle growth than those prepared by sol–gel route. On the basis of XRD, FT-IR, XPS and ^{29}Si MAS-NMR, a strong interaction was found between SiO_2 and TiO_2, and Ti–O–Si bonds formed during both the two routes. But more Ti–O–Si bonds formed in the composite nanoparticles prepared by sol–gel-hydrothermal route than those prepared by sol–gel route. As a result, the titania–silica composite nanoparticles prepared by sol–gel-hydrothermal route exhibited higher photocatalytic activity in decomposition of methylene blue than that prepared by sol–gel route, and it had excellent photocatalytic activity even after calcined at 1000 °C.

Keywords: Titania; Silica; Sol–gel; Hydrothermal; Nanoparticles; Photocatalytic

1. Introduction

Nano-sized titania has attracted increasing attention because of its wide applications in many fields, such as catalysts and supports, ceramics, inorganic membranes, sensors, solar energy conversion and so on [1–4]. In particular, recently numerous works have been carried out to display its photocatalytic activity due to its promising performance in degrading various organic and inorganic environmental pollutants [5–7]. Properties influencing the photocatalytic activity of titania particles have been reported to include surface area, crystallinity, crystallite size and crystal structure [8,9]. Typically, the photocatalytic activity of amorphous titania is negligible, and anatase shows higher photocatalytic activity than rutile. It is generally accepted that anatase titania nanoparticles with high crystallinity and large specific surface area are desirable in photocatalytic reactions.

However, the rutile phase is thermodynamically stable and the anatase phase is metastable. The transformation from anatase to rutile can occur during heating or even mechanical grinding. The addition of LaO_2 [10], CeO_2 [11], CuO [12], Fe_2O_3 [13], SiO_2 [14–17] or other oxides into anatase titania can improve the thermal stability and photoactivity. Among them, silica–titania composite nanoparticles has been reported to exhibit high thermal stability, quite larger surface area and a better photocatalytic performance than pure titania. Such materials are thus considered a potential candidate as photocatalyst [15–17].

The most widely used methods to synthesize silica–titania composite nanoparticles are sol–gel method

*Corresponding author. Fax: +86 351 4041 153.
E-mail address: yhsun@sxicc.ac.cn (Y. Sun).

0022-4596/$ - see front matter © 2004 Elsevier Inc. All rights reserved.
doi:10.1016/j.jssc.2004.12.034

[15,18–21], co-precipitation [22–25] and chemical vapor deposition [26]. The sol–gel method is most widely used due to its possible capability in controlling the textural and surface properties of composite oxides. This method is mainly based on the hydrolysis and polycondensation of a metal alkoxide, which ultimately yields hydroxide or oxide under certain conditions. To obtain homogeneous macromolecular oxide networks for qualified nanomaterials in sol–gel processing, control of hydrolysis is essentially important. In these methods, sol–gel-derived precipitates are amorphous in nature. So calcination in air is inevitable for the transformation from amorphous to anatase phase. But the calcination process frequently lead to serious particle agglomeration, grain growth, small surface area and phase transformation from anatase to rutile, which all decrease the photocatalytic activity of titania. The hydrothermal processing represents an alternative to the calcination for the crystallization of titania under mild temperatures. It has been widely applied in the synthesis of zeolites and in the production of advanced ceramic powders with ultrafine particle size. In the hydrothermal treatment, grain size, particle morphology, crystalline phase, and surface chemistry can be controlled via processing variables such as sol composition, pH, reaction temperature and pressure, aging time, and nature of solvent and additive. Typically, under various hydrothermal conditions, products of TiO_2 with different morphologies and microstructural forms have been yielded [27,28]. It provides a facilitated route to prepare a uniform, dispersed, and well-crystalline anatase titania nanoparticles. However, to the best of our knowledge, the sol–gel-hydrothermal method has not been used for the preparation of titania–silica composite nanoparticles. It is well known that the method of preparing titania–silica nanoparticles determines its physico-chemical and photocatalytic properties and the effects of silica on titania are quite different from the synthetic procedures, so the comparative study on the properties of titania–silica nanoparticles prepared by different routes is necessary.

Thus, the present work was carried out to compare the physico-chemical and photocatalytic properties of titania–silica composite nanoparticles prepared by sol–gel and sol–gel-hydrothermal routes, respectively. The results demonstrated that titania–silica composite nanoparticles prepared by sol–gel-hydrothermal route showed higher thermal stabilities and better photocatalytic activity than that by sol–gel route.

2. Experimental section

2.1. Synthesis of samples

In the present work, titanium *n*-butoxide (TB) and tetraethoxysilane (TEOS) were used as titanium and silica sources, respectively. The typical synthetic procedure follows the preparation of titanta–silica nanoparticles scheme in Fig. 1.

In the first step, TEOS was added to 55 ml of 2 M HNO_3 solution at 50 °C with magnetic stirring and a sol was formed. 17 ml TB was then added dropwise to the above sol under magnetic stirring within 0.5 h. Then the hydrolysis product was stirred for 1 h to form a gel. The gel was treated by the following two routes, respectively.

Sol–gel process: The gel was transferred into oven, and treated at 50 °C for 24 h. Then it was dried at 120 °C. Finally, the powders were further calcined at 400 °C in air for 2 h. Then the titania–silica composite nanoparticles were obtained. The products were denoted as SG-series.

Sol–gel-hydrothermal process: After aged for 0.5 h at 20 °C, the gel loaded into a Teflon-lined autoclave for hydrothermal reaction at 140 °C for 10 h. After that, the hydrothermal product was dried at 120 °C. Then the titania–silica composite nanoparticles were obtained. The products were marked SGH-series.

According to the SiO_2 content defined as $SiO_2\% = W_{SiO_2}/(W_{SiO_2} + W_{TiO_2}) = 0$, 3.5, 7.0, 15.0, 40.0, 60.0, 80.0, and 100 wt%, where W meant weight of SiO_2 or TiO_2 in products, the products were designed as SG0, SG1, SG2, SG3, SG4, SG5, SG6, SG7 for SG series and SGH0, SGH1, SGH2, SGH3, SGH4, SGH5, SGH6, SGH7 for SGH series, respectively. To further study, the samples were calcined at 400, 600, 800 and 1000 °C in air for 2 h.

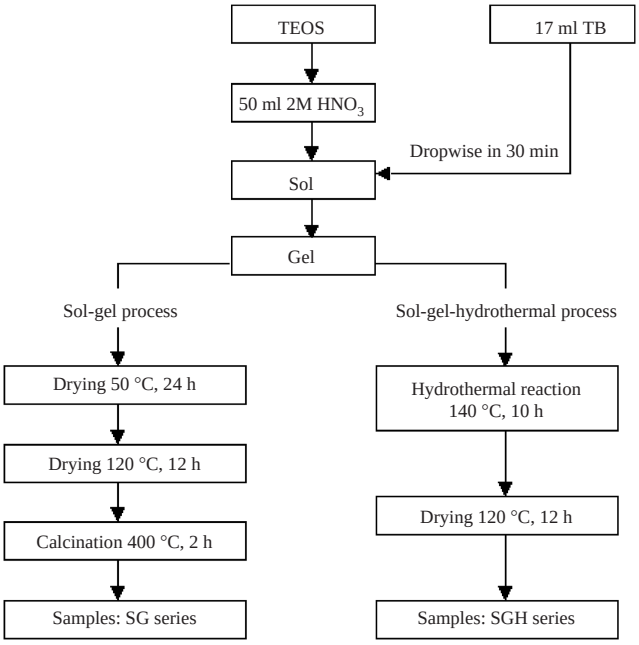

Fig. 1. Preparation of titania–silica nanoparticles.

2.2. Characterization of samples

The crystalline phase and the phase transformation of titania particles were determined by X-ray diffraction (XRD, Cu$K\alpha$, 40 kV, 100 mA, D/max2500 Rigaku). The fraction of rutile phase presenting in the samples were calculated using the following Eq. (1):

$$\text{Rutile}\% = 1/[1 + 0.8(I_A/I_R)], \quad (1)$$

where, I_A and I_R are the X-ray integrated intensity of (101) reflection of anatase and (110) reflection of rutile, respectively. The crystallite grain size was estimated according to Scherrer formula (2):

$$L = K\lambda/(\beta \cos \theta), \quad (2)$$

where λ is the wavelength of the X-ray radiation (Cu$K\alpha = 0.15406$ nm), K is a constant taken as 0.89, β is the line width at half-maximum height, and θ is the diffracting angle.

The morphologies of the titania–silica composite nanoparticles were observed with transmission electron microscope (TEM, Hitachi-600-2) and high-resolution transmission electron microscopy (HRTEM, JEOL-2010, with an accelerating voltage of 200 kV). The element composition and the chemical state of particle surface were determined by X-ray photoelectron spectroscopy (XPS, Mg$K\alpha$ as radiation source, PHI5300X, Perkin-Elmer Physics Electronics). The BET surface area was measured by nitrogen adsorption at 77 K (Tristar3000, Micromeritics). The chemical structure information of the particles was collected by FT-IR spectra (Nicolet 560 Spectrometer) and ^{29}Si MAS-NMR spectra (Varian Infinity Plus spectrometer). Diffuse reflectance spectra (DRS) recorded by a Shimadzu UV-2101 apparatus, equipped with an integrating sphere, using $BaSO_4$ as reference.

2.3. Photodecomposition of methylene blue (MB)

The photochemical reactor consisted of a cylindrical jacketed quartz tube with 5.0 cm in diameter and 27 cm in length. A highly pressure mercury vapor lamp of 300 W was placed inside the reactor. To keep temperature of the solution during the reaction, water was circulated through the annulus of the jacket quartz tube. The light source assembly was placed concentrically inside the 300 ml Pyrex glass container of 6.0 cm in diameter and 28.5 cm height filled with 250 ml MB solution. The distance between the source and bottom of the vessel was 1.5 cm to aid for better stirring using a magnetic stirrer. The radiated wavelength of lamp was predominantly at 365 nm. The MB original concentration was 100 ppm. The catalyst loading was 0.5 kg/m^3 of TiO_2. In all experiments, prior to irradiation, the suspension of TiO_2 catalyst in MB solution was stirred in the dark for 30 min to ensure adsorption/desorption equilibrium. The concentration of MB at this point was used as the initial value for the further kinetic treatment of the photodecomposition process. Samples were collected from the reactive system at regular intervals and centrifuged to analyze by the UV-Vis spectrophotometer to determine the concentration of MB.

3. Results and discussion

3.1. Thermal stability of titania–silica composite nanoparticles

The XRD patterns of titania–silica composite nanoparticles and the crystalline properties are shown in Fig. 2 and Table 1, respectively. The addition of silica significantly influenced the phase transition of titania. Pure rutile phase was directly synthesized by SGH route without silica addition (see SGH0 in Fig. 2a). However, after a little silica was introduced into the reaction system, no rutile phase could be produced (see

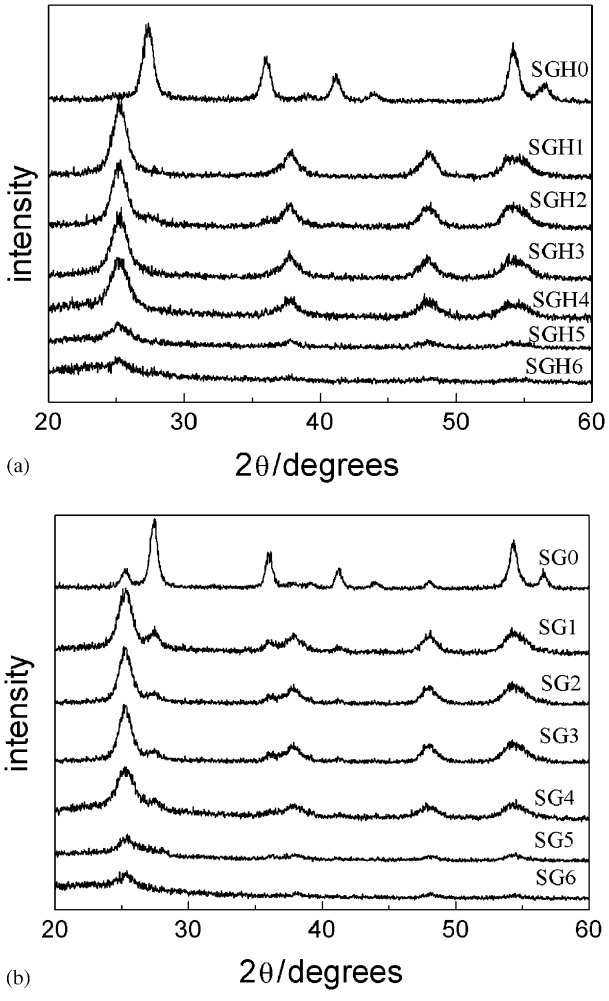

Fig. 2. XRD patterns of the titania–silica composite nanoparticles: (a) SGH-series and (b) SG-series.

Table 1
Physical properties of the titania–silica composite nanoparticles

SiO_2 (wt%)	SG-series				SGH-series			
	Samples	Structure		Grain size[a] (nm)	Samples	Structure		Grain size[a] (nm)
		Anasase (%)	Ruitle (%)			Anasase (%)	Ruitle (%)	
0	SG0	22	78	20.7	SGH0	0	100	—
3.5	SG1	57	43	13.4	SGH1	100	0	13.8
7.0	SG2	71	29	12.1	SGH2	100	0	11.9
15.0	SG3	90	10	11.8	SGH3	100	0	9.3
40.0	SG4	95	5	8.1	SGH4	100	0	7.0
60.0	SG5	96	4	6.8	SGH5	100	0	4.9
80.0	SG6	100	0	6.0	SGH6	100	0	4.0

[a]Grain size is of anatase phase.

SGH1–SGH6 in Fig. 2a). Furthermore, the anatase titania grain size decreased from 13.8 to 4.0 nm with the increase of silica content (see Table 1). For SG-series samples, the anatase and rutile phases coexisted until the silica content was higher than 60%, although the content of anatase increased with the increase of silica amount. Also, the grain sizes of the samples decreased from 20.7 to 6.2 nm (see Table 1). In addition, no peaks for the silica crystal phase were observed for all samples from both preparing methods, which meant that silica existed absolutely as an amorphous phase in the titania–silica composite nanoparticles. Because of the interference of amorphous SiO_2 with TiO_2 lattice, the crystallinities of the titania–silica composite nanoparticles were worse than that of pure TiO_2.

These results suggested that the crystallinity and grain sizes of the titania–silica composite nanoparticles prepared by both methods depended on the silica content and silica inhibited the formation of rutile phase and the growth of crystal grain. Moreover, for SGH route, the addition of a little silica (3.5 wt %) could prevent the formation of rutile phase and the growth of grain size, suggesting that SGH route was more effective to prepare anatase titania–silica composite nanoparticles compared with SG route.

In order to establish a possible crystallization process of titania by increasing the temperature, XRD analysis was carried out on the samples calcined at 120, 400, 600, 800 and 1000 °C, respectively. Typical diffraction patterns obtained from samples of SG2, SG4, SGH2 and SGH4 are shown in Fig. 3. It is well known that calcinations can improve the crystallinity of the sample, and that anatase phase will change to rutile phase at special calcination temperature. So the temperature at which rutile phase begins to form is generally used to characterize the thermal stability of the titania. It can be seen that the SG2 dried at 120 °C already showed weak peaks of anatase and rutile phases (see Fig. 3a). Subsequently, the gradual transformation from anatase to rutile occurred when heated from 120 to 1000 °C. Finally, at 1000 °C, the SG2 was completely rutile phase. Compared to SG2, the phase transformation of SG4 was far difficult because of the more silica in composite particles, but some rutile phase still formed (see Fig. 3b) after 800 °C. On the other hand, for the SGH series, the addition of silica showed more significant inhibiting effect on the rutile phase formation. There appeared very little rutile phase for SGH2 and no rutile phase for SGH4 even calcined until 1000 °C (see Fig. 3c, d).

It is clear that the titania–silica composite nanoparticles prepared by SGH process had better thermal stability against the phase transformation from anatase to rutile than that from SG process. This result suggested that SGH route led to better atomically mixed structure between TiO_2 and SiO_2, which retarded the phase transformation to the rutile and the polycrystallization due to the possible strong bonding of Ti–O–Si linkage. Therefore, this high thermal stability made it possible to calcine the titania–silica composite nanoparticles at higher temperature without the formation of the rutile phase and to prepare highly crystallinzed particles with reducing the bulk defects.

The TEM images of pure TiO_2 (SG0 and SGH0) treated at 120 and 400 °C are presented in Fig. 4. The average particle sizes of pure titania increased rapidly with the increase of calcination temperature. After calcined at 400 °C for 2 h, the SG0 aggregated markedly and the average particle size increase to 25.0 nm. The SGH0 was aciculae, which was the shape of rutile phase, and it increased from 35 to 50 nm after calcined at 400 °C for 2 h.

The TEM images of SGH4 and SG4 calcined at different temperatures for 2 h are presented in Figs. 5 and 6, respectively. Obviously, the nanoparticles of SGH4 (Fig. 5c) were well dispersed and held at around 10.0 nm at 800 °C for 2 h. Especially after calcined at 1000 °C, the particle size was around 17 nm and very uniform, only slight agglomeration occurred. This indicated the sintering process of titania–silica composite nanoparticles prepared by SGH could be effectively

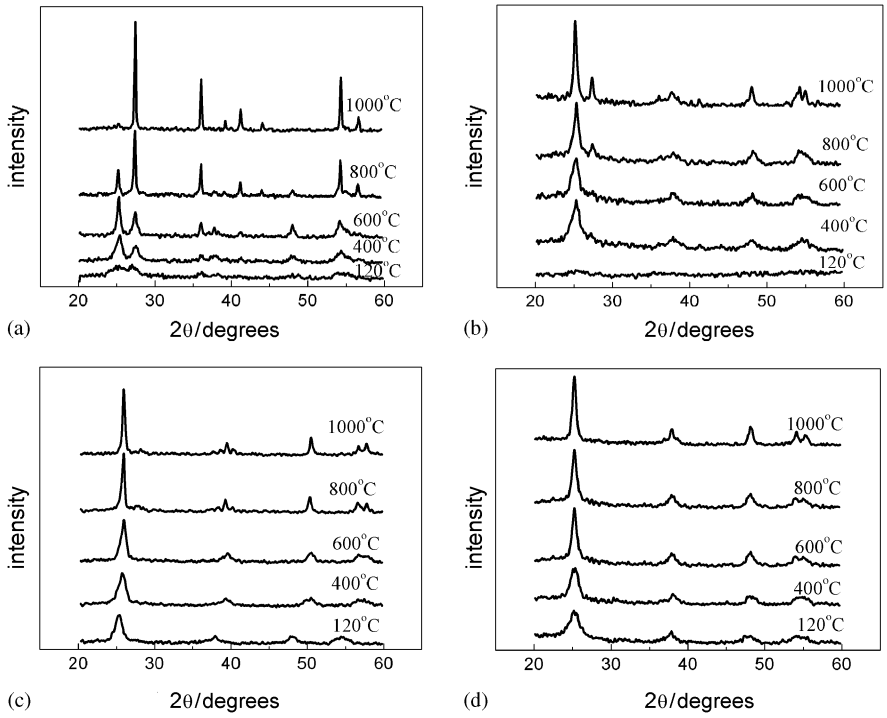

Fig. 3. XRD patterns of the titania–silica composite nanoparticles calcined at different temperatures for 2 h: (a) SG2, (b) SG4, (c) SGH2 and (d) SGHS4.

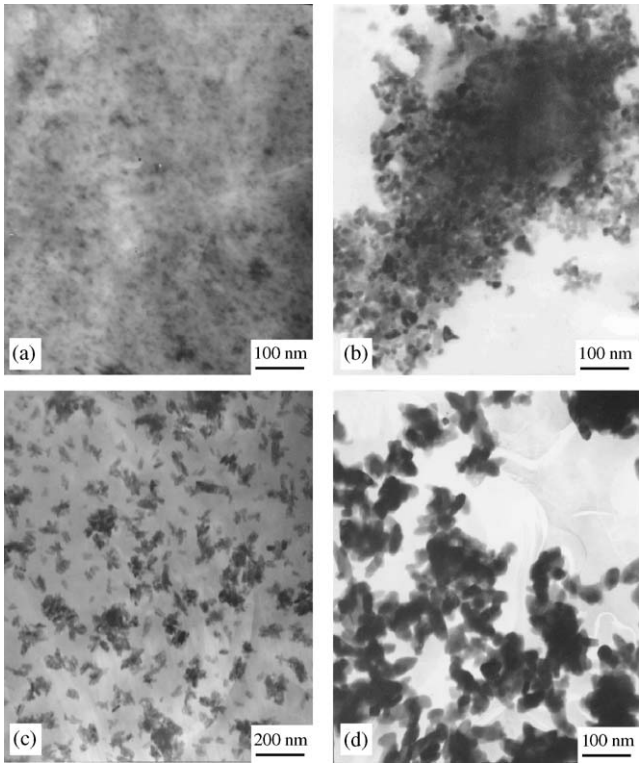

Fig. 4. Transmission electron micrographs of the titania–silica composite nanoparticles: (a) SG0 (treated at 120 °C), (b) SG0 (treated at 400 °C), (c) SGH0 (treated at 120 °C) and (d) SGH0 (treated at 400 °C).

retarded through the addition of silica at high temperature. Unfortunately, sample SG4 began its agglomeration when calcined at 400 °C (Fig. 6b). After calcined above 800 °C, the SG4 was obviously sintered and some large particles appeared (Fig. 6d). HRTEM images of SGH4 and SG4 were shown in Fig. 7. It proved that the sizes of crystal were smaller than 10 nm with calcined at 400 °C for 2 h.

Nitrogen adsorption measurements of these samples were performed as an alternative method to judge their thermal stability. The BET surface areas of the samples calcined at different temperature were listed in Table 2. It can be seen that the surface areas were strongly dependent on the thermal-treating temperature and silica content. The surface areas of the two pure TiO_2 samples decreased drastically after calcined at 400 °C. However, the titania–silica composite nanoparticles possessed rapidly increasing surface area with the increase of silica content. Even after calcined at 800 °C, SG4 and SGH4 remained high surface area of 152.0 and 216.8 $m^2 g^{-1}$, respectively. This result indicated that the addition of amorphous silica into titania matrix suppressed the reduction of surface area and the suppression was more effective at higher silica content.

The surface areas of SGH-series decreased more slowly than SG-series when they were calcined from 120 to 800 °C for 2 h in air. Especially, SGH4 and SGH6 retained unexpected large surface areas of 129.7 and

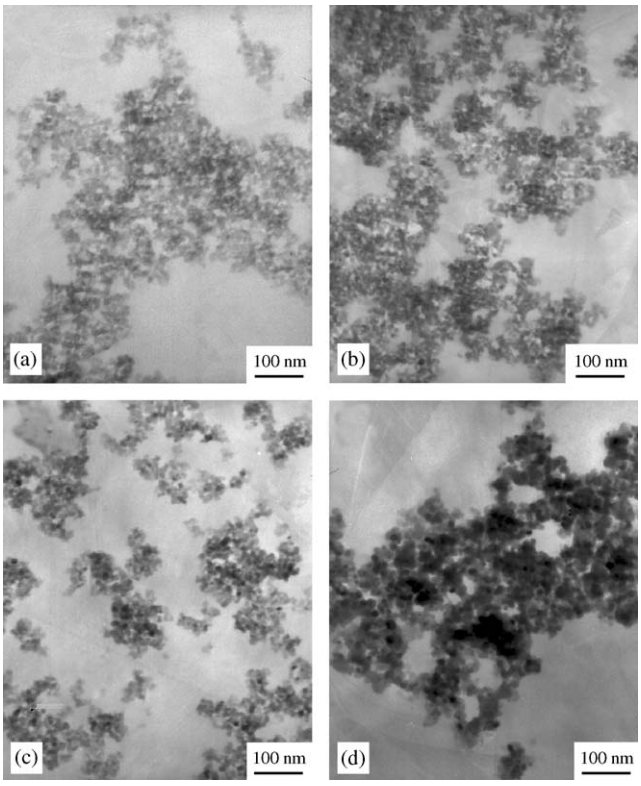

Fig. 5. Transmission electron micrographs of SGH4 calcined at different temperature in air for 2 h: (a) 120 °C, (b) 400 °C, (c) 800 °C and (d) 1000 °C.

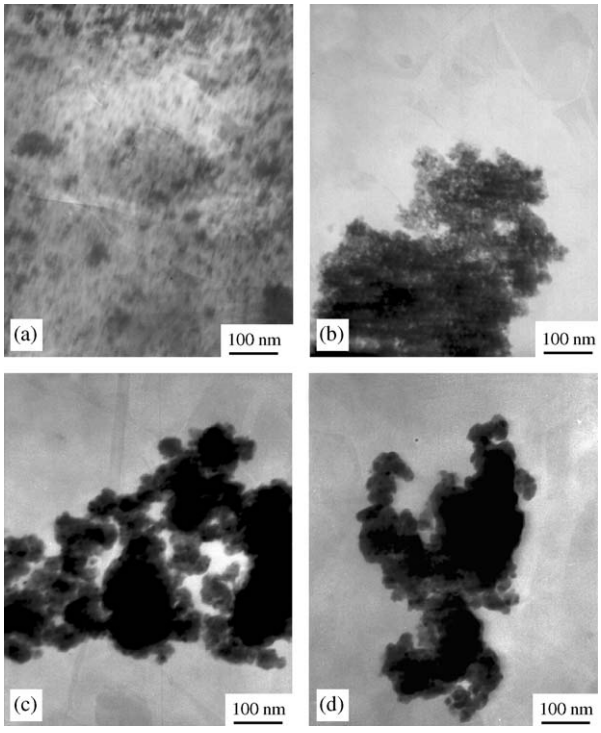

Fig. 6. Transmission electron micrographs of SG4 calcined at different temperature in air for 2 h: (a) 120 °C, (b) 400 °C, (c) 800 °C and (d) 1000 °C.

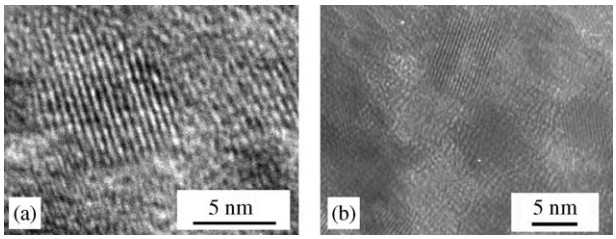

Fig. 7. HRTEM images of samples calcined at 400 °C in air for 2 h: (a) SGH4 and (b)SG4.

Table 2
The BET surface areas of the pure titania and titania–silica composite nanoparticles calcined at different temperature

Sample	SiO_2 content (wt%)	Surface area ($m^2 g^{-1}$)				
		120 °C	400 °C	600 °C	800 °C	1000 °C
SG0	0	112.3	12.8	—	—	4.8
SG1	3.5	238.8	143.2	71.0	32	4.3
SG4	40	406.2	374.2	245.2	152.0	9.4
SG6	80	464.4	574.7	455.1	252.1	0.6
SGH0	0	95.0	21.0	—	—	7.8
SGH1	3.5	131.6	152.7	96.2	—	8.9
SGH4	40	181.6	254.7	246.1	216.8	129.7
SGH6	80	735.5	830.2	780.9	660.6	215.7

215.7 $m^2 g^{-1}$, respectively even after calcined at 1000 °C. But for the SG-series samples, the surface areas of SG4 and SG6 were decreased markedly to less than 10 $m^2 g^{-1}$ after calcined at 1000 °C for 2 h.

Thermal stability plays an important role in many potential applications of nano-materials. It is well known that conventional titania nanoparticles exhibits low thermal stability. In detail, the nanoparticles agglomerate into large clusters, the surface area simultaneously decreases, and the anatase phase transforms into the rutile phase with an increase of calcination temperature [29,30]. Here, the results from XRD, TEM and BET surface areas revealed higher thermal stability from SGH route than from SG route. Hence, it suggested that the interaction between SiO_2 and TiO_2 was stronger in SGH-series than in SG-series.

In pure titania, the experimental observation that the anatase-to-rutile phase transformation begins at the surface of the bulk anatase is related to the high tangential diffusion of anatase nanopheres deduced by molecular dynamics simulations [31]. It is widely accepted that the presence of silica can retard the transformation of anatase to rutile phase and keep the surface area of anatase through the Ti–O–Si interaction [15,18,19]. At the interface, some Ti atoms replace Si atoms in the tetrahedral SiO_2 lattice to form tetrahedral Ti sites. The interaction between the tetrahedral Ti species and the octahedral Ti sites in the anatase is thought to prevent the transformation from anatase to

rutile. The SiO_2 lattice locks the Ti–O species at the interface with the TiO_2 domains and prevents the nucleation that is necessary for the phase transformation to rutile. On the other hand, small crystallite size played thermodynamically in favor of anatase instead of rutile, due to the differences in surface energy and surface stress [32]. So, besides the Ti–O–Si interface, the small crystallite size of titania–silica composite nanoparticles should also contribute to retarding transformation from anatase to rutile.

3.2. The formation of Ti–O–Si bonds in titania–silica composite nanoparticles

Fig. 8 shows the FT-IR transmission spectra of titania–silica composite nanoparticles calcined at 600 °C for 2 h, only the most interesting region (1600–400 cm^{-1}) of specific bands for titania–silica mixture. In all spectra, the absorption peaks around 1620 cm^{-1} were attributed to bending mode of hydroxyl. It is generally admitted that titania strongly retains adsorbed undissociated water due to the strong Lewis acidity of the co-ordinatively unsaturated Ti^{4+} surface sites [33]. Ti–O–Ti vibration appeared in the range of 400–600 cm^{-1} as the result of condensation reaction. For titania–silica composite nanoparticles, the peak at 800 cm^{-1} corresponded to the symmetric stretching vibration of Si–O–Si. And the peaks at 1087 or 1110 cm^{-1} corresponded to the asymmetric stretching vibration of Si–O–Si. Theoretically, it is possible to distinguish two types of interaction between TiO_2 and SiO_2: physically mixed (weak Van der Waals forces) and chemically bonded (formation of Ti–O–Si linkages). The simplest way to examine the formation of Ti–O–Si bonds is to use IR spectroscopy. The IR band observed at 910–960 cm^{-1} might be due to the stretching vibration band of Ti–O–Si bonds [31,32,34]. So the wave number at 930–960 cm^{-1} in the spectra of the titania–silica composite nanoparticles prepared by both routes indicated the possibility of formation of bonds of Ti–O–Si. And the higher the content of SiO_2 was in the composite nanoparticles, the more intensive this peak was. In summary, FT-IR spectra confirmed that prepared composite nanoparticles might be chemically bonded materials.

The binding energy and nominal surface atomic concentration of pure TiO_2, SG4 and SGH4 are listed in Table 3. It also revealed the strong interaction between TiO_2 and SiO_2 in the samples. Compared to that of pure TiO_2, the binding energy (O1*s*, Ti2$p_{1/2}$ and Ti2$p_{3/2}$) of the SG4 increased by about 1.7, 2.0 and 1.8 eV, respectively. For SGH4, the binding energy of O1*s*, Ti2$p_{1/2}$ and Ti2$p_{3/2}$ increased by about 1.9, 2.1 and 2.2 eV. The chemical shifts of binding energy for elements resulted from the extent of valence electron shielding of core electrons from nuclear charge and this

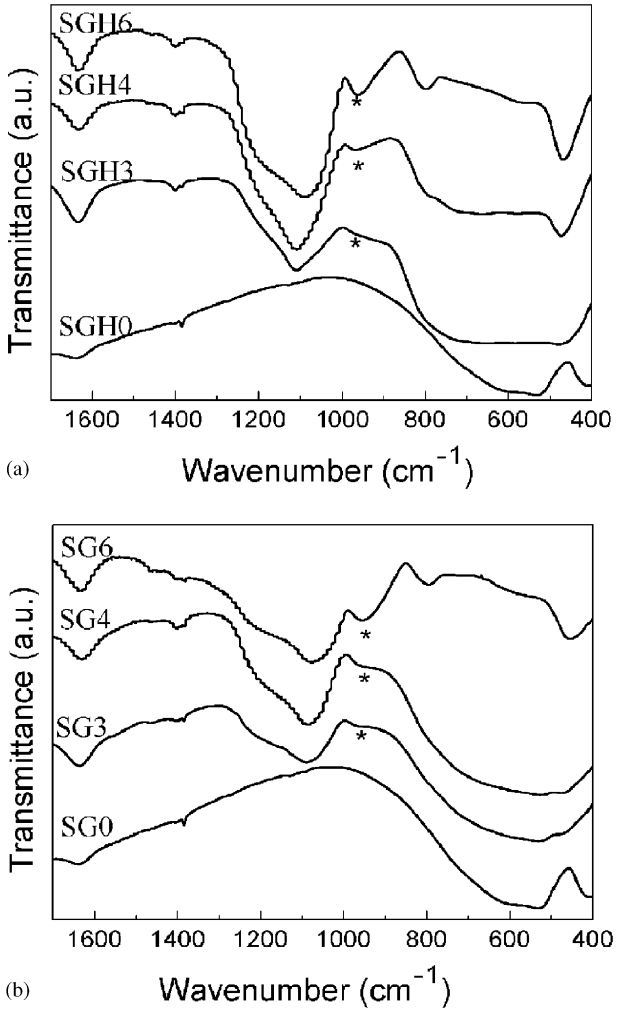

Fig. 8. The FT-IR transmission spectra of the pure titania and titania–silica composite nanoparticles calcined at 600 °C in air for 2 h: (a) the SGH-series and (b) the SG-series (* Ti–O–Si vibration).

shift was an indicator of the oxidation state. The shift in O1*s* peak might be due to the interaction of highly electropositive Ti with Si–O–Si bond. Thus the Si–O–Si bond was replaced by Ti–O–Si bond. The Ti–O bond might then be more ionic in character, making the oxygen atom more negative [25,35].

XPS analyses also showed the nominal surface atomic percentages of Si and Ti did not correspond to the percentages in the composite samples, and the surface appeared enriched in silica. This showed good agreement with the results of Pabon et al. [18]. The high concentration of Si on the surface should also interfere with the diffusion and sintering of anatase nanoparticles during calcination.

The ^{29}Si MAS NMR spectra were used to study the evolution of the local environment around Si atoms in the titania–silica composite nanoparticles. Fig. 9 shows the ^{29}Si MAS NMR spectra for SG4 and SGH4 calcined at 600 °C for 2 h. After peak separation, three NMR

Table 3
Binding energy of O1*s*, Ti2*p*, Si2*p* and the surface atomic concentration of samples

Samples	O1*s*		Ti2$p_{1/2}$		Ti2$p_{3/2}$		Si2*p*		Added atomic[a] (%)		Nominal surface atomic (%)	
	BE	FWHM	BE	FWHM	BE	FWHM	BE	FWHM	Si	Ti	Si	Ti
TiO_2	532.0	2.00	466.2	2.38	460.4	1.86	—	—	0	100	0	100
SG4	533.7	1.96	468.2	2.09	462.2	1.98	107.1	2.15	47.1	52.9	79.0	21.0
SGH4	533.9	2.06	468.3	2.09	462.6	1.96	107.4	2.18	47.1	52.9	78.4	21.6

BE means binding energy (eV). FWHM means full-wave at halfmaximum.
[a]The added atomic concentration is calculated from the weight composition.

peaks were defined as Q^4, Q^3 and Q^2, where Q denoted the silicon atom; the superscript 4, 3, or 2 meant the number of Si–O–Si bridges connecting to Q. So the NMR peaks of Q^2 and Q^3 were thought to be equivalent to two or one –OTi groups around Si, suggesting the insert of Ti^{4+} into the amorphous SiO_2 phase of the titania–silica composite nanoparticles. The relative amounts of these different Si species derived from the integrated areas of their peaks are listed in Table 4. For SG4, Q^3 was dominant and Q^4 sites was only 4.66%, indicating that there were only fractional complete Si–O–Si tetrahedrons and the most of Si in SGH4 had –OTi or –OH groups around them. So there was a higher degree of Ti substitution in the silica lattice, indicating extensive formation of Si–O–Ti bonds, or there was extensive formation Si–O–H. However, for SG4, the percent of Q^4 is 48.86% (see Table 4), indicating that the silica had relatively well-developed three-dimensional tetrahedrons than SGH4.

More accurately, the mean number of bridging Si–O–Si bonds can also be expressed by the AFS parameter [36], which calculated using Eq. (3):

$$\mathrm{AFS} = \frac{\sum_{i=1}^{i=4} iS^i}{\sum_{i=1}^{i=4} S^i}, \tag{3}$$

where S^i is the integrated area corresponding to NMR peak Q^i and i is the number of Si–O–Si around Si atom. The titania–silica composite nanoparticles SG4 had an AFS of 3.11 and 2.98 for SGH4. So it was clear that there were more Si–O–Si formed in the titania–silica composite nanoparticles prepared by SG route than that by SGH route.

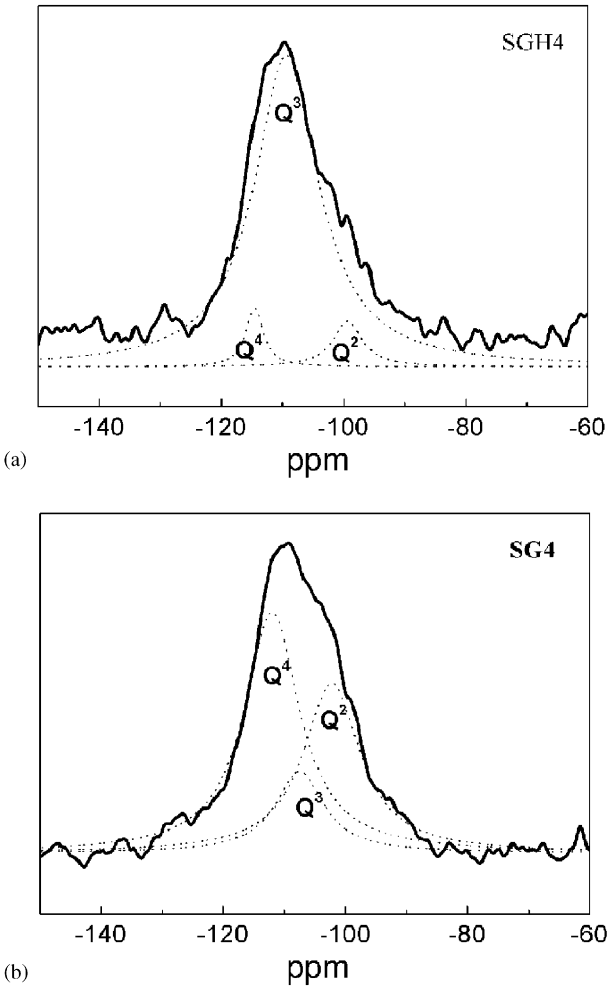

Fig. 9. The ^{29}Si single-pulse solid-state MAS NMR spectra for SGH4 and SG4 calcined at 600 °C for 2 h.

3.3. UV-Vis absorption and photodegradation of MB in water by titania–silica nanoparticles/UV

The diffuse reflectance spectra of pure TiO_2 and titania–silica composite nanoparticles were shown in Fig. 10. The spectra showed a blue shift in the absorbing band edge with the increasing silica amount. The band edge blue shift of DRS spectra was resulted from the well-known quantum size effect of semiconductors [37] and the band-gap difference between anatase and rutile phase. According to size quantization, an increase in the band-gap happened with the decrease in particle dimensions, and the increased band-gap led to a blue shift in the absorption spectrum [38]. In the two crystal structures, the anatase phase has larger energy band-gap ($E_g = 3.23$ eV), but rutile phase has a smaller one ($E_g = 3.02$ eV) [39]. With the increase of the silica content, the proportion of anatase percent increased in SG-series, resulting in the gradual blue shift of absorp-

Table 4
The relative amounts of different structural sites derived from the integrated areas of ^{29}Si single-pulse solid-state MAS NMR

Samples	Q^4		Q^3		Q^2	
	ppm	%	ppm	%	ppm	%
SG4	−110.9	48.86	−107.1	14.56	−102.6	36.57
SGH4	−114.0	4.66	−109.9	89.28	−100.8	6.08

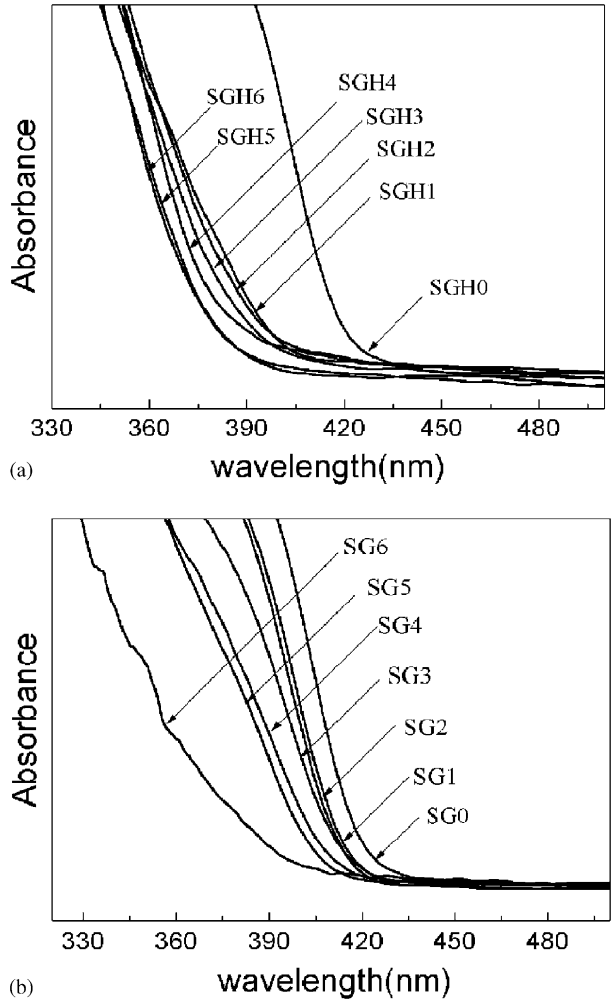

Fig. 10. The DRS of pure TiO_2 and titania–silica nanoparticles: (a) SGH-series samples and (b) SG-series samples.

tion band edge. Because all titania–silica composite nanoparticles in SGH-series was anatase phase and the pure TiO_2 is rutile phase, all titania–silica composite nanoparticles blue shifted largely from that of pure TiO_2.

Compared the DRS spectra, it can be see that the SGH-series had larger band-gap than SG-series. With the increase of the band-gap of the nano-sized TiO_2 particles, the oxidizing potential of the photon generated

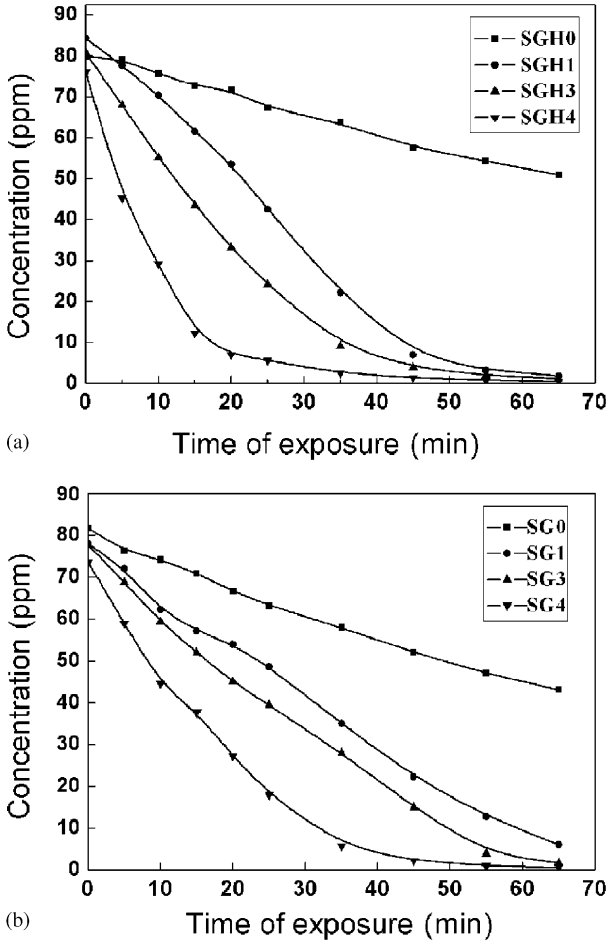

Fig. 11. Kinetics of the photocatalytic decomposition of MB: (a) SGH-series and (b) SG-series.

holes (h^+) and the reducing potential of the photon-generated electrons (e^-) will increase. Therefore, titania–silica composite nanoparticles prepared by SGH route should possess high photooxidation ability as well as photoreduction capabilities.

The strong oxidizing potential of the photogenerated holes made titania–silica composite nanoparticles one of the most attractive photocatalysts for oxidation [40–42]. Fig. 11 gives kinetics of the photocatalytic decomposition of MB. For both series, approximately 20% MB was adsorbed by catalyst before reaction. The titania–silica composite nanoparticles showed a better photocatalytic activity than that of pure TiO_2 nanoparticles (SG0 or SGH0) and the higher silica content led to the better photocatalytic activity in titania–silica composite nanoparticles. Apparently, the photocatalytic activity of SGH-series samples was higher than that of SG-series samples prepared with the same silica content. As shown in Fig. 12, the SGH4 showed excellent photocatalytic activity even after calcined at 1000 °C, but the SG4 behaved very low photocatalytic activity. So the titania–silica composite nanoparticles by SGH route

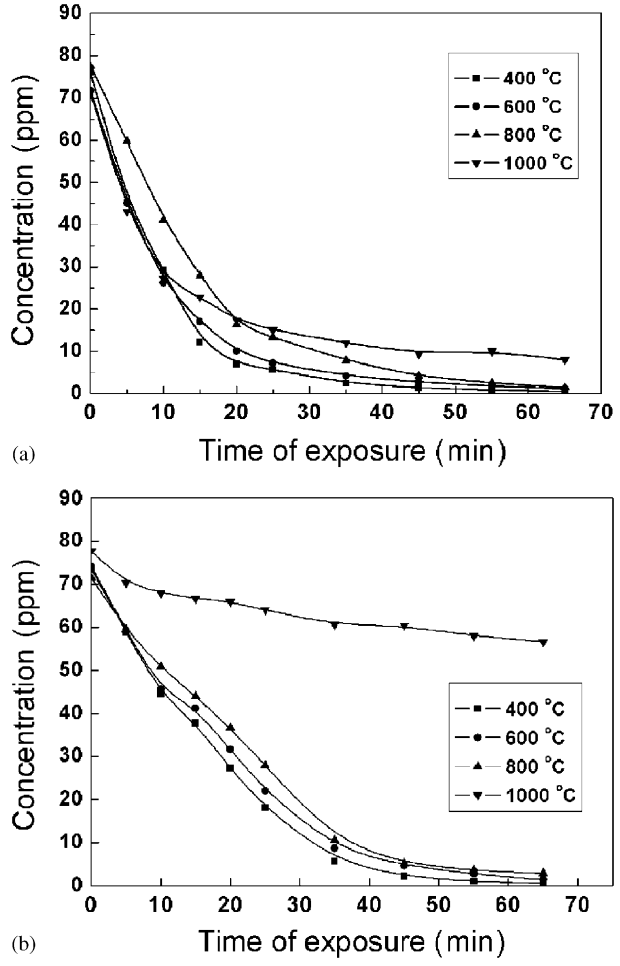

Fig. 12. Kinetics of the photocatalytic decomposition of MB on samples calcined at different temperature for 2 h: (a) SGH4 and (b) SG4.

was far more promising as highly thermal stable photocatalyst produced than SG route.

4. Conclusion

Titania–silica composite nanoparticles were prepared by SGH route and SG route, respectively. There was strong interaction between SiO_2 and TiO_2 in titania–silica composite nanoparticles, and Ti–O–Si bonds formed during both the two routes. Due to the strong interaction of SiO_2 and TiO_2, titania–silica composite nanoparticles showed an improved thermal stability against the phase transformation from anatase to rutile, agglomeration of particles and the growth of particles. Compared with the SG-series samples, the SGH-series samples had better thermal stability. Even calcined at 1000 °C, the SGH4 with 40 wt% silica still possessed stable anatase phase, large specific surface area of 129.7 m^2/g and small particles average size of 17 nm. On the contrast, the SG4 with 40 wt% silica was a mixture of anatase and ruitle phase, and the particles was sintered with surface area of 9.4 $m^2 g^{-1}$. As a result, on the photocatalystic decomposition MB experiment, the SGH-series samples had better excellent photocatalytic activity than the SG-series samples, and it showed excellent photocatalytic activity even after calcined at 1000 °C. So the titania–silica composite nanoparticles prepared by SGH route were a more promising photocatalyst than that prepared by SG route.

Acknowledgment

The work is supported by National Native Science Foundation of China (Grant No. 20133040).

References

[1] B.M. Reddy, I. Ganesh, V.R. Reddy, J. Mater. Sci. Lett. 17 (1998) 1913–1915.
[2] L. Miao, P. Jin, K. Kaneko, A. Terai, N. Nabatova-Gabain, S. Tanemura, Appl. Surf. Sci. 212 (2003) 255–263.
[3] A.K. Ray, S.M. Tracey, S.N.B. Hodgson, J. Sol–Gel Sci. Technol. 22 (2001) 15–22.
[4] S.K. Poznyak, V.I. Pergushov, A.I. Kulak, C.W. Schlapfer, J. Phys. Chem. B 103 (1999) 1308–1315.
[5] A.F. Popa, P.H. Mutin, André Vioux, G. Delahayb, B. Coqb, Chem. Commun. (2004) 2214–2215.
[6] E. Traversa, M.L.D. Vona, P. Nunziante, S. Licoccia, J.W. Yoon, T. Sasaki, N. Koshizaki, J. Sol–Gel Sci. Technol. 22 (2001) 115–123.
[7] K.T. Ranjit, H. cohen, I. Willner, S. Bossmann, A.M. Braun, J. Mater. Sci. 34 (1999) 5273–5280.
[8] B. Zielinska, J. Grzechulska, B. Grzmil, A.W. Morawski, Appl. Catal. B 35 (2001) L1–L7.
[9] B. Ohtani, Y. Ogawa, S. Nishimoto, J. Phys. Chem. B 101 (1997) 3746–3752.
[10] C.P. Sibu, S. Rajesh Kumar, P. Mukundan, K.G.K. Warrier, Chem. Mater. 14 (2002) 2876–2881.
[11] M.S.P. Francisco, V.R. Mastelaro, Chem. Mater. 14 (2002) 2514–2518.
[12] J.C.S. Wu, H. Tseng, W.C. Chang, J. Nanopart. Res. 3 (2001) 113–118.
[13] C.Y. Wang, D.W. Bahnemanna, J.K. Dohrmannb, Chem. Commun. (2000) 1539–1540.
[14] K.Y. Jung, S.B. Park, J. Photochem. Photobiol. A 127 (1999) 117–122.
[15] S.R. Kumar, C. Suresh, K.A. Vasudevan, N.R. Suja, P. Mukundan, K.G.K. Warrier, Mater. Lett. 38 (1999) 161–166.
[16] I.W. Tanakulrungsamk, M. Inoue, J. Mater. Sci. Lett. 19 (2000) 1439–1443.
[17] C. Anderson, A.J. Brad, J. Phys. Chem. B 101 (1997) 2611–2616.
[18] E. Pabon, J. Retuert, R. Quijiada, A. Zarate, Micropor. Mesopor. Mater. 67 (2004) 195–203.
[19] X. Fu, L.A. Clark, Q. Yang, M.A. Anderson, Environ. Sci. Technol. 30 (1996) 647–653.
[20] G. Dagan, S. Sampath, O. Lev, Chem. Mater. 7 (1995) 446–453.
[21] C. Anderson, A.J. Bard, J. Phys. Chem. 99 (1995) 9882–9885.
[22] P.K. Doolin, S. Alerasool, D.J. Zalewski, J.F. Hoffman, Catal. Lett. 25 (1994) 209–212.
[23] C.B. Khouw, C.B. Dartt, J.A. Labinger, M.E. Davis, J. Catal. 149 (1994) 195–205.

[24] B.M. Reddy, E.P. Reddy, B. Manohar, Appl. Catal. A 96 (1993) L1–L5.
[25] A.Y. Stakheev, E.S. Shpiro, J. Apijok, J. Phys. Chem. 97 (1993) 5668–5672.
[26] V.M. Gun'ko, V.I. Zarko, V.V. Turov, R. Leboda, E. Chibowski, L. Holysz, E.M. Pakhlov, E.F. Voronin, V.V. Dudnik, Yu.I. Gornikov, J. Colloid Interface Sci. 198 (1998) 141–156.
[27] Yu.V. Kolen'ko, V.D. Maximov, A.V. Garshev, P.E. Meskin, N.N. Oleynikov, B.R. Churagulov, Chem. Phys. Lett. 388 (2004) 411–415.
[28] Yu.V. Kolen'ko, B.R. Churagulov, M. Kunst, L. Mazerolles, C. Colbeau-Justin, Appl. Catal. B 54 (2004) 51–58.
[29] Y. Tanaka, M. Suganuma, J. Sol–Gel Sci. Technol. 22 (2001) 83–89.
[30] A.M. Ruiz, G. Dezanneau, J. Arbiol, A. Cornet, J.R. Morante, Chem. Mater. 16 (2004) 862–871.
[31] X. Gao, I.E. Wachs, Catal. Today 51 (1999) 233–254.
[32] H. Zhang, Banfield, J. Mater. Chem. 8 (1998) 2073–2076.
[33] B.A. Morrow, in: J.L.G. Fierro (Ed.), Spectroscopic Characterization of Heterogeneous Catalysis, Elsevier Science Publishers, Amsterdam, 1990, p. A161.
[34] S. Kein, S. Thorimbert, W.F. Maier, J. Catal. 163 (1996) 476–488.
[35] S.M. Mukhopadhayay, S.H. Garofalini, J. Noncryst. Solids 126 (1990) 202–208.
[36] C. Mutter, T.N.M. Bernards, M.P.J. Peeters, J.H. Lammers, M.R. Bohmer, Thin Solid Films 351 (1999) 95–98.
[37] M. Anpo, T. Shima, S. Kodama, Y. Kobokawa, J. Phys. Chem. 91 (1987) 4305–4310.
[38] K.M. Reddy, C.V.G. Reddy, S.V. Manorama, J. Solid. State Chem. 158 (2001) 180–186.
[39] S.J. Kim, E.G. Lee, J. Sol–Gel Sci. Technol. 22 (2001) 63–74.
[40] K.M. Reddya, S.V. Manorama, A.R. Reddyb, Mater. Chem. Phys. 78 (2002) 239–245.
[41] D.A. Panayotov, D.K. Paul, J.T. Yates, J. Phys. Chem. B 107 (2003) 10571–10575.
[42] T.V. Nguyen, O.B. Yang, Catal. Today 87 (2003) 67–79.